

Dalton Transactions

Accepted Manuscript



This is an *Accepted Manuscript*, which has been through the Royal Society of Chemistry peer review process and has been accepted for publication.

Accepted Manuscripts are published online shortly after acceptance, before technical editing, formatting and proof reading. Using this free service, authors can make their results available to the community, in citable form, before we publish the edited article. We will replace this *Accepted Manuscript* with the edited and formatted *Advance Article* as soon as it is available.

You can find more information about *Accepted Manuscripts* in the [Information for Authors](#).

Please note that technical editing may introduce minor changes to the text and/or graphics, which may alter content. The journal's standard [Terms & Conditions](#) and the [Ethical guidelines](#) still apply. In no event shall the Royal Society of Chemistry be held responsible for any errors or omissions in this *Accepted Manuscript* or any consequences arising from the use of any information it contains.

Molecular simulation of low temperature argon adsorption in several models of IRMOF-1 with defects and structural disorder

L. Sarkisov^a

Abstract. Defects and inclusions in metal-organic frameworks (MOFs) have captured attention of the scientific community as a possible new source of interesting functionalities. Currently, little is known about how presence of defects and guest molecules affects adsorptive, catalytic, mechanical and other properties of a MOF crystal and there is a clear need for a comprehensive theoretical framework. In this article we offer several conceptual models of IRMOF-1 with defects and guest molecules and explore properties of these models using computational structure characterization methods and molecular simulation of argon adsorption at 78 K.

Introduction

In the last 15 years metal-organic frameworks (MOFs), aside from being promising materials for a number of applications, kept challenging our perception of what is possible, in terms of properties and behaviour, in the world of porous materials¹. MOFs with ultrahigh surface areas² and MOFs capable of large volume changes as a result of some external stimuli while remaining crystalline³ are just two examples of new and intriguing phenomena. Another feature of MOFs is their sheer number and diversity, resulting simply from the vast library of organic chemistry. This prompted a conjecture that for each application in question, from sensing, adsorption and catalysis to sorting and drug delivery, there is a MOF, either already synthesized or yet-to-be-synthesized, with properties ideal for this specific application. This in turn changed the way we approach material optimization, with a significant emphasis now placed on large-scale computational screening of real and virtual structures⁴.

So far, in all these developments, both theoretical and experimental, MOFs have been treated as ideal, defect-free crystals. And yet, there is no such thing as an ideal crystal: all real crystals, to some extent, contain various types of defects and impurities, although techniques to grow *nearly* perfect crystals have been perfected over the years. In MOFs, it has been now recognized, defects are pervasive and may include missing linkers, partially collapsed frameworks, interpenetrated frameworks or regions, trapped molecules of solvent and building components, pores and regions of porous space blocked and inaccessible to adsorbates and so on. One may rather rely on an operational definition of an ideal crystal, as the crystal whose adsorption and other properties relevant for a specific application cannot be distinguished from a defect-free structure within the accuracy of an experimental measurement.

There has been a substantial recent interest in classification, characterization and control of these defects in MOFs⁵. Indeed, for some applications, such as photonics, it is important to have as perfect crystal as possible and growing high quality crystals has become an important field in itself. Small structural imperfections in MOFs may serve as a source mechanical and

^a Institute for Materials and Processes, School of Engineering, The University of Edinburgh

chemical instability, ultimately leading to degradation of the material, an issue well known and endemic for MOFs. Yet, a new line of thought looks at these defects as a source of original functionalities and unexpected phenomena, particularly in catalysis, adsorption and crystal mechanics⁶.

How do adsorptive, catalytic, mechanical and other properties of MOFs depend on the presence of defects, their type and concentration? This is an emerging area of a substantial theoretical and practical interest.

One important aspect in the development of the approaches within this area is to recognize that presence of defects in MOFs makes them disordered structures. From this point of view there are other closely related systems, where the disorder of the structure comes not from the structural defects of the underlying crystal and faults in the synthetic procedure, but from a deliberate introduction of an additional component to the system and post-synthetic modification of the ligands.

Molecular simulations could be of an extreme value in the emerging field of defect-engineering in MOFs as in simulations behaviour of systems with defects and disordered systems can always be compared to a reference, defect-free structure, based on the crystallographic data.

The idea of this conceptual article is to explore how some of these defects and structural disorder in MOFs can be modelled and what type of deviations in structural characteristics, such as accessible surface area and porosity, and properties one might expect from the presence of the defects and disorder.

As a model structure we consider a well-known and one of the earliest reported MOFs, IRMOF-1, also known as MOF-5⁷. In this preliminary study we will focus on structural characteristics and adsorption properties explored through argon sorption at 78 K.

Methodology

All simulations in this study are carried out using the energy biased grand canonical Monte Carlo method (GCMC), as implemented in the MuSiC simulation package⁸. Further details of the GCMC simulation protocol adopted in this work, including the number of Monte Carlo moves per adsorption point, type and weight of Monte Carlo moves and other parameters, are provided in the Supplemental Information file (SI) file.

For all species (IRMOF-1, argon, dimethylformamide (DMF) and gold nanoclusters) we adopt the Universal Force Field (UFF) interaction parameters⁹, summarized in the SI file. We will comment on the pitfalls of using “off-the-shelf” force fields in later sections. The Lennard-Jones (LJ) cross-species interactions are calculated using the standard Lorentz-Berthelot mixing rules. All LJ interactions are truncated at the cut-off distance of 12.8Å with no long-tail corrections applied. All species, including the adsorbent IRMOF-1 are treated as rigid. Electrostatic contribution to the total interaction energy is considered for the case of

DMF and gold nanoclusters (interacting with their own molecules and with IRMOF-1). Partial charges on the atoms of metal-organic frameworks are taken from the work of Yazaydin *et al.*¹⁰ For DMF, partial charges are calculated using the B3LYP Density Functional Theory method¹¹⁻¹³, with 6-31G basis set and CHELPG charge analysis¹⁴ using the Gaussian 09 software package¹⁵. Fluid-fluid electrostatic interactions between partial charges are calculated using the Fennell-Gezelter method¹⁶ based on a spherically truncated summation (at 12.8Å), while in the solid-fluid case the Ewald summation is applied¹⁷. All solid-fluid interactions are pre-calculated using a cubic lattice with 0.2 Å resolution and stored as potential maps prior to the adsorption simulations. In all cases we consider a system of 2x2x2 replicas of the IRMOF-1 unit cell as the adsorbate system. In all cases we consider only one realization of the system due to computational constraints. A more robust study should consider all properties (adsorption isotherms, surface area etc) averaged over multiple realizations of structural disorder.

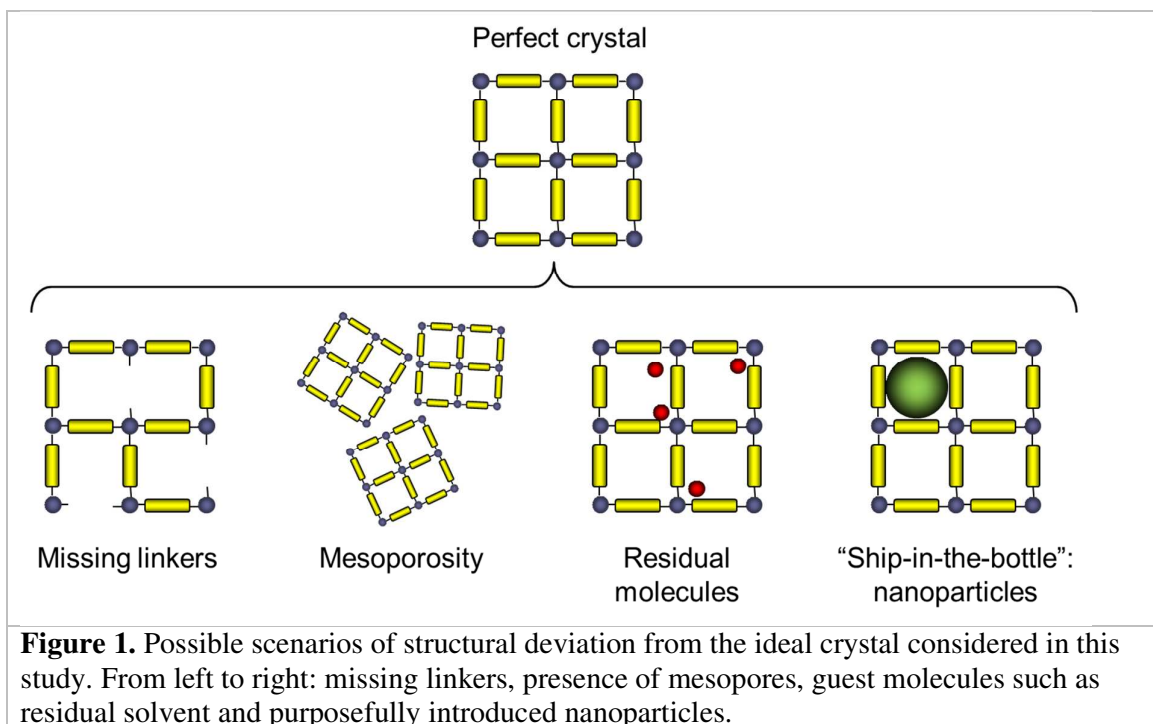
Saturation pressure of argon as described by the UFF parameters is calculated using the revised Lennard-Jones equation of state¹⁸.

Structural characteristics of the systems, including surface area, pore volume, pore size distribution are obtained with the Poreblazer v3.0.2 simulation suite, using the methods summarized in our previous publication¹⁹. Energy barriers for transport of gold nanoclusters within IRMOF-1 are estimated using the methodology reported in our previous work^{20, 21}.

All isotherms are reported in mg/g units consistent with the available experimental data and previous simulation studies²². Other technical details pertaining construction of the specific systems will be provided as needed in relevant sections.

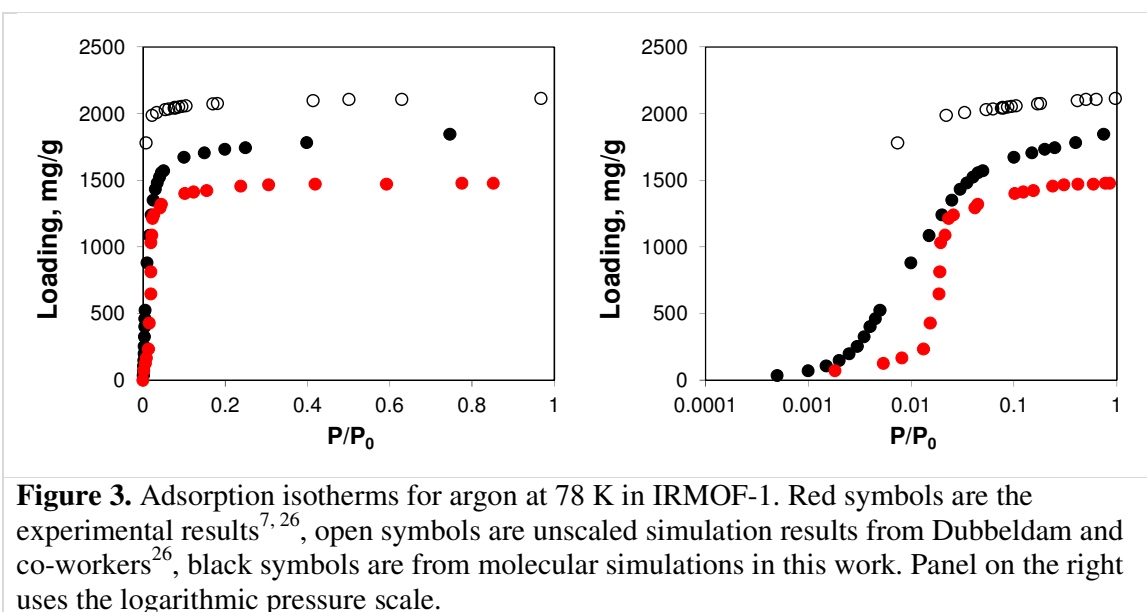
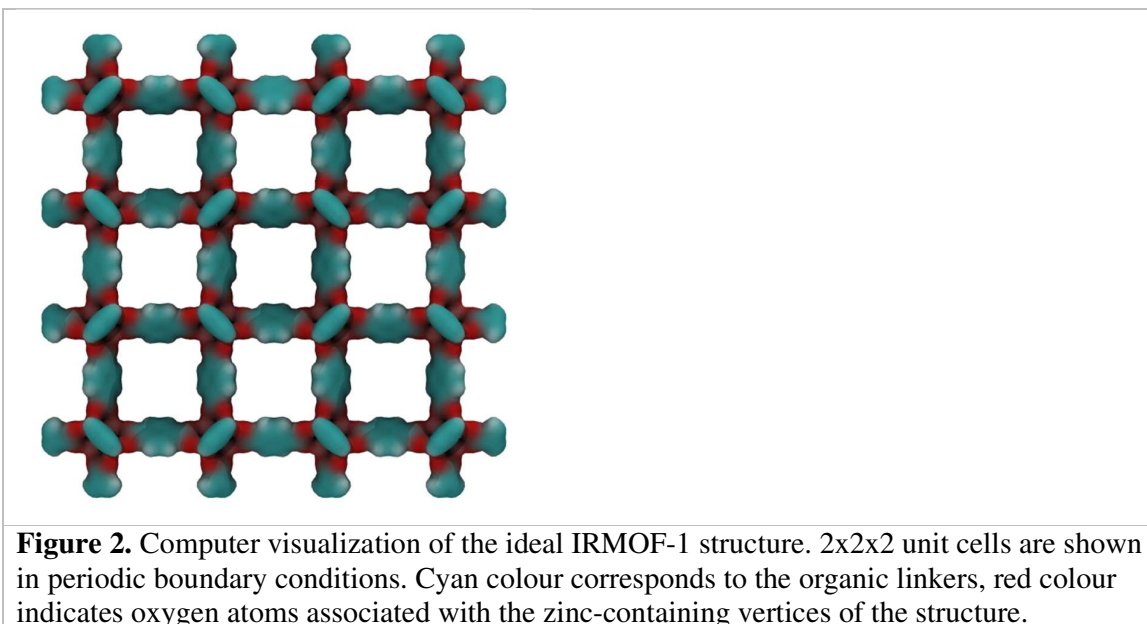
Results

The types of deviations from the perfect structure of IRMOF-1 we consider in this work are summarized in Figure 1 and include missing linkers, regions of mesoporosity between nanocrystalline regions, presence of solvent molecules and IRMOF-1 structures loaded with gold nanoclusters. This is, of course, not an exhaustive list of all possible deviations of the structure from the perfect crystal (and, likely, we do not know yet all possible types of defects that can exist in MOFs). For example we do not consider systems with post-synthetic modification of the linkers²³ or so called multivariate MOFs²⁴, while not all of the scenarios considered here are directly relevant for IRMOF-1. This will be further commented on as we present the individual cases.



Before we consider structural features and adsorption behaviour of these modified IRMOF-1 structures, it is important to establish behaviour of the reference, perfect crystal.

Figure 2 shows the molecular visualization of the IRMOF-1 crystal (2x2x2 unit cells). The structure consists of two alternating cages of about 11.37 ± 0.20 Å and 14.62 ± 0.20 Å in diameter, connected by windows of 7.71 ± 0.20 Å (the pore limiting diameter). The accessible surface area is estimated at 3381.49 m²/g, which agrees well with experimentally reported values (for example, 3534 m²/g²⁵). Figure 3 reports adsorption isotherms from molecular simulations and experiments. The experimental data by Li *et al.*⁷, was also presented in the work of Dubbeldam and co-workers²⁶, who extensively investigated locations and types of sites available for light gases within IRMOF-1. Here we report the amount adsorbed in the units consistent with those studies.



As can be seen from Figure 3, molecular simulations over-predict IRMOF-1 capacity for argon. This is consistent with the studies by Dubbeldam and co-workers (although in their work, simulated capacity was ~40% higher than in experiments, whereas here it is ~20% higher than in experiments), who associated this with a portion of the structure being blocked and inaccessible to the adsorbate molecules²⁶. The differences between the two sets of the simulation results are likely associated with the choice of the force field for the framework and argon. On the right of Figure 3 we also re-plot the same adsorption isotherm using the logarithmic scale for pressure. The shift of the simulated isotherm to lower values compared

to the experiments suggests stronger solid-fluid interactions in the model, compared to the real structure.

Let us now consider the case where some of the linkers are missing in IRMOF-1. Experimentally, there is now sufficient amount of evidence that MOFs with missing linkers do exist, and moreover can be created on purpose^{5,27,28}. For example, Zhou and co-workers have prepared variants of NOTT-101 material with missing linkers, by using a combination of the actual linkers and linker fragments in the synthesis²⁹. The resulting structures featured larger pore volume and even mesopores. It then leads to some interesting questions as to how much of the linkers should be removed from the structure to induce mesoporosity, how this threshold depends on the MOF and ligands and whether the resulting structures are mechanically stable. In another example, MOFs based on zirconium and carboxylate linkers are known to feature missing linkers and, in fact, these defects can be induced via modification of the synthetic procedure²⁷. As has been recently discussed by Cliffe *et al.*, the defects in UiO-66 structure seem to aggregate in defect-rich regions and these phenomena requires some further explanation and understating³⁰.

Using IRMOF-1 as a basic model, we consider the effect of the portion of the linkers removed. Here the ligands are removed by cleaving the bonds between the sp² carbon of the terephthalic acid linker and oxygen atoms. We acknowledge here that from the chemical perspective it is unrealistic and more physically meaningful models can be constructed, including those for the NOTT-101 and UiO-66 materials. Using Poreblazer structure analysis tools¹⁹, we ensure that the remaining structures still form fully supported, percolated cluster. Figure 4 plots surface areas and geometric pore size distributions (PSDs) as a function of the percentage of linkers removed. Indeed, the surface area (in m²/g) steadily increases with the number of linkers removed. The pore size distribution remains almost identical to the perfect crystal up to 20% of linkers removed (so these PSDs are not shown), however at 50% linkers removed, the PSD starts to develop new peaks, closer to the mesoporous region and at 65% and 73% more of these peaks are added at the positions clearly dictated by the topology of the MOF itself and the characteristic vertex-vertex distances.

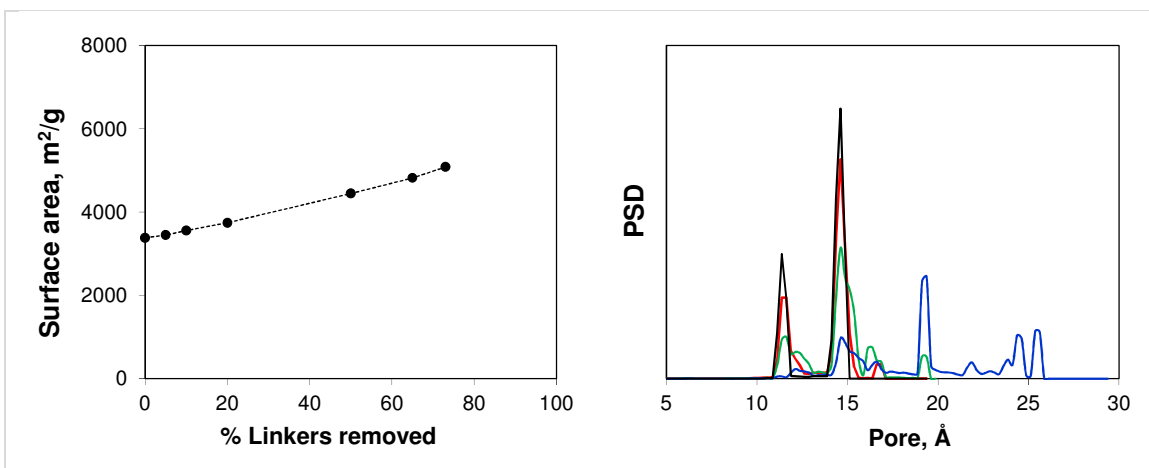


Figure 4. On the left: accessible surface area (m²/g) in IRMOF-1 as a function of the percentage of linkers removed. Line is for eye guidance, only. On the right: geometric pore

size distribution as a function of the percentage of linkers removed. Black line is for 0% (perfect crystal), red line is for 50%, green line is for 65% and blue line is for 73% linkers removed, respectively.

Adsorption isotherms in the defected structures in comparison with the reference simulation and experimental results are shown in Figure 5.

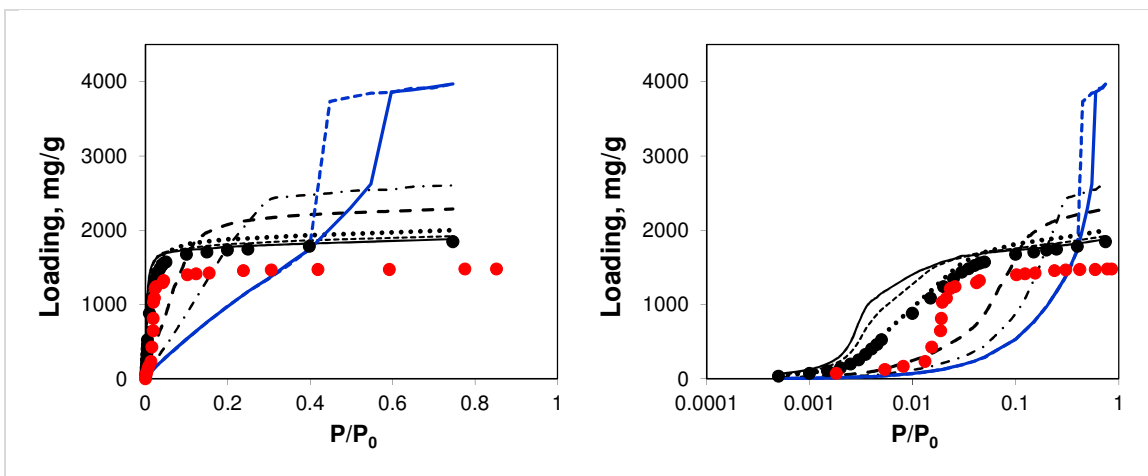
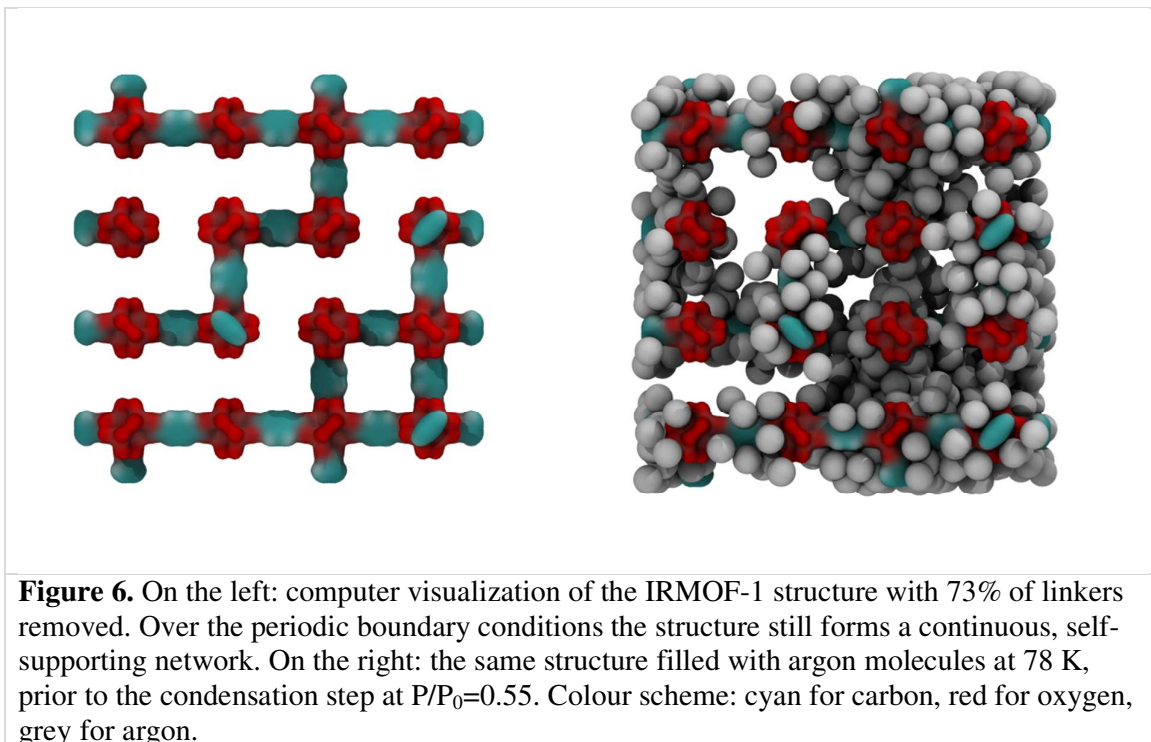


Figure 5. Argon adsorption isotherms at 78 K in IRMOF-1 structures with progressively larger proportion of linkers removed. Red symbols are the experimental results^{7,26}, black symbols are from molecular simulations for the perfect crystal. Solid black line is for 5%, short dash line is for 10%, dot line is for 20%, long dash line is for 50%, dot-dash line is for 65% and blue line (solid line for adsorption, dash line for desorption) is for 73% of linkers removed, respectively. The panel on the right plots the same data, using the logarithmic pressure scale.

Small number of linkers removed (5%, 10%, and 20% solid line, short dash, and dot lines, respectively) lead to essentially the same simulated isotherm as for the perfect crystal with slightly larger capacity and stronger interactions in the low pressure regime. This is particularly evident for the case of 20% of linkers removed. The real change becomes more visible at 50% of linkers removed (long dash line) with the isotherm levelling at much greater loading value and featuring much less steep initial slope of the isotherm due to the weakened solid-fluid interactions. This trend continues for 65% of linkers removed, however no signs of capillary condensation or hysteresis behaviour are yet observed. At 73% of linkers removed, the isotherm has a completely different shape, corresponding to an intermediate case between Type IV and V isotherm and featuring a hysteresis loop, associated with the presence of the mesopores as observed from the PSD. This is similar to the mesoporosity emerging in NOTT-101 as a result of incorporation of incomplete linkers, as reported by Park *et al.*²⁹. However, Park and co-workers did not observe such a dramatic impact on the initial slope of the isotherms as in the simulations here, suggesting that in their materials mesopores form in between reasonably intact microporous domains. We will consider an alternative model capturing this situation.

Figure 6 shows the IRMOF-1 structure with 73% of linkers removed and the same structure with argon molecules adsorbed right before the capillary condensation step.



There are other possible scenarios of how mesoporosity can occur or introduced into a MOF structure. For example, Choi *et al.* showed that synthesis of IRMOF-1 in the presence of carefully controlled amounts of 4-(dodecyloxy)benzoic acid (DBA) leads to a sponge-like structure, with pores of 10 nm – 100 nm incorporated into the crystalline structure of IRMOF-1, as evidenced from scanning electron microscopy (SEM) and powder X-ray diffraction (PXRD) analysis³¹. Interestingly, characterization via nitrogen adsorption at 77 K produced adsorption isotherms of Type I for sponge structures, very similar in shape to the isotherm for the reference microcrystalline IRMOF-1, but with lower capacity for nitrogen. Mesoporous materials would be expected to have Type IV or V adsorption isotherm with a characteristic hysteresis loop³². At least in the case of one of the sponge-like materials, the authors offered an interpretation of these results, whereas liquid-like nitrogen in micropores blocks access to the large interior cavities. We believe that other alternative explanations are also possible: the interior cavities may not be fully evacuated (which would explain lower capacity for nitrogen) and the pores are too large in size (in the macroporous region) and therefore condensation takes place very close to $P/P_0=1$ to lead to a proper Type IV adsorption isotherm.

Molecular simulations can help in interpreting this type of experimental work by constructing hypothetical models of mesoporosity in MOFs and exploring their behaviour. Here, we investigate just one variant of the model of this type, where a single mesopore of 20 Å in size is introduced into the microcrystalline structure of IRMOF-1. For this we consider sheets of

IRMOF-1 crystal of two unit cells wide (51.338 \AA) separated by a 20 \AA gap in x direction, as schematically depicted in Figure 7. In x direction, the crystal is cut between the sp^2 carbons and aromatic rings and exposed sp^2 carbon atoms are capped with hydrogen atoms to preserve correct valence.

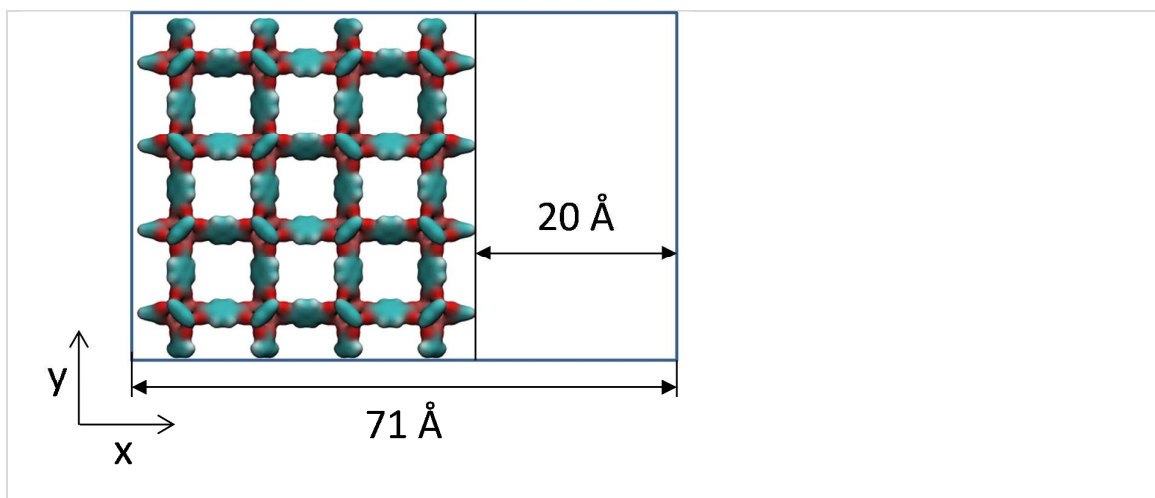


Figure 7. Schematic depiction of a mesoporous model of IRMOF-1 considered here. In x direction the system consists of alternating sheets of IRMOF-1 crystal of two unit cells wide and gaps of 20 \AA wide. The system is in periodic boundary conditions in y and z directions.

Adsorption behaviour of this system is shown in Figure 8 in comparison with the perfect crystal, experimental data and the mesoporous system obtained by removing 73% of linkers.

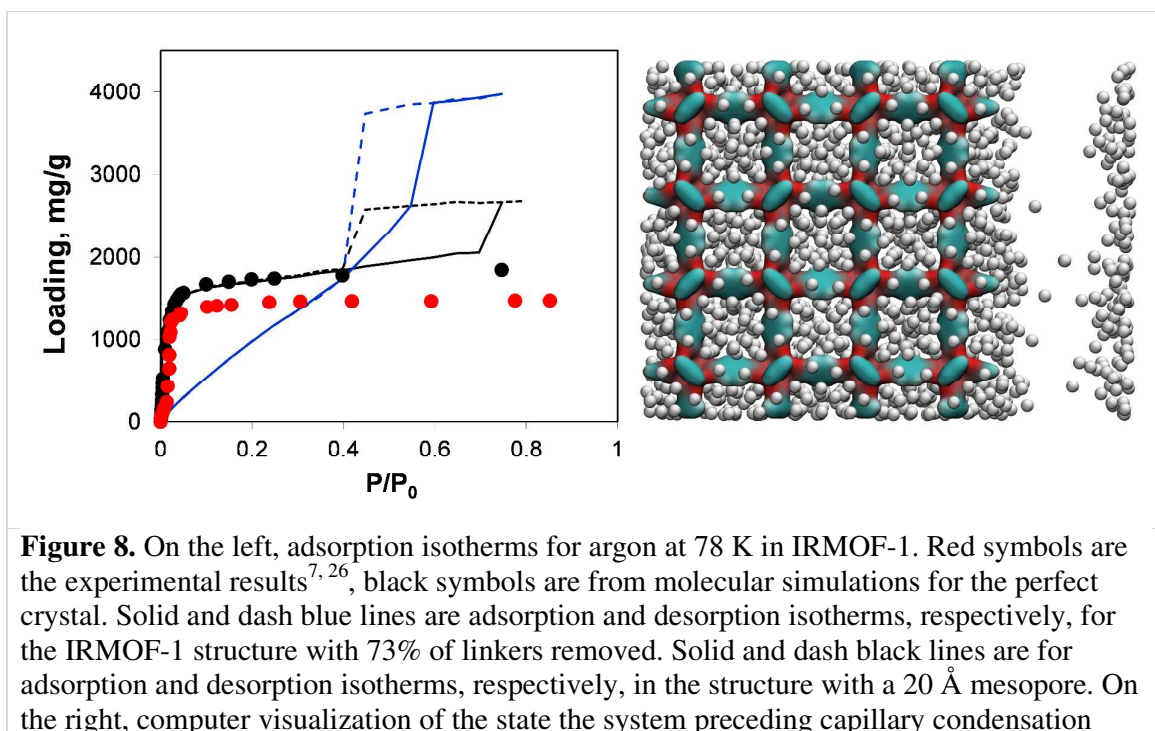


Figure 8. On the left, adsorption isotherms for argon at 78 K in IRMOF-1. Red symbols are the experimental results^{7, 26}, black symbols are from molecular simulations for the perfect crystal. Solid and dash blue lines are adsorption and desorption isotherms, respectively, for the IRMOF-1 structure with 73% of linkers removed. Solid and dash black lines are for adsorption and desorption isotherms, respectively, in the structure with a 20 \AA mesopore. On the right, computer visualization of the state the system preceding capillary condensation

step. The colour scheme is as before. Argon particles are scaled down in size for better visualization.

Indeed, presence of a single mesopore induces formation of a hysteresis loop (with the system behaving essentially as a slit pore with complex walls). This isotherm can be classified as Type IV and it is quite different from the isotherm obtained via removal of a large number of linkers: as expected at lower pressures its behaviour essentially retraces the microporous behaviour of the pristine IRMOF-1, with the contribution of the mesopore switched on at a higher pressure. For the system based on the removed linkers, it is the very structure of the microporous IRMOF-1 that has been substantially altered, leading to the weak solid-fluid interactions and large porosity. In fact, the model featuring a single mesopore seems to reflect more closely a situation where defects induced by missing linkers also aggregate, with the resulting pores coalescing into larger mesopores. From this perspective, the isotherm reported in Figure 8 for the model with 20 Å mesopore is qualitatively much closer to the results of Park *et al.*²⁹, which serves as indirect evidence of the defect aggregation.

Loading MOFs with guest molecules has been considered as an attractive route to create new, emergent properties for catalysis, sensing and other applications³³. Aside from modifying MOF properties in this way on purpose, residual solvent and building components will also change adsorption and other properties of a MOF structure, compared to a fully evacuated, perfect crystal. Influence of guest solvent molecules on adsorption properties of IRMOFs (and in particular on adsorption of carbon dioxide at 298 K) has been previously studied by Bae and co-workers³⁴. They argued, based on the results of the thermogravimetric analysis (TGA), that about 3.5 wt % of solvent remained in the variant of IRMOF-16 they investigated after evacuation. In our system, this corresponds to about 3 DMF molecules per unit cell of IRMOF-1. Here we investigate adsorption of argon at 78 K in the IRMOF-1 system containing residual DMF molecules. The SI file provides structural characteristics of these systems, such as surface area and porosity. Firstly, as can be seen in Figure 9, DMF prefers to occupy energetically favourable locations in the corner of the structure.

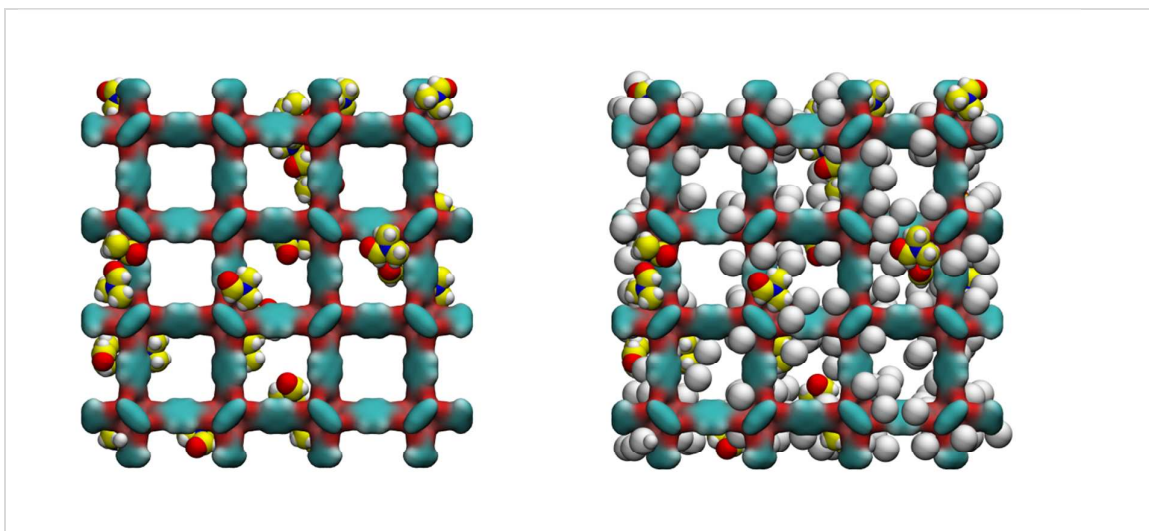


Figure 9. On the left: computer visualization of IRMOF-1 structure loaded with 24 molecules of DMF. On the right: the same structure shown together with the adsorbed argon molecules. Colour scheme: in IRMOF-1 cyan is for carbon, red for oxygen, grey for argon; for DMF, nitrogen is blue, carbon is yellow, oxygen is red and hydrogen is grey.

As can be seen from the adsorption isotherms, presence of residual solvent molecules reduces the volume of the system; it also reduces slightly the accessible surface area and pore limiting diameter (see SI). At low pressures, although DMF occupies energetically favourable positions, that otherwise would be occupied by argon molecules, overall, it provides an additional contribution to the adsorption energy, shifting the isotherm to lower pressures, compared to the reference ideal crystal case.

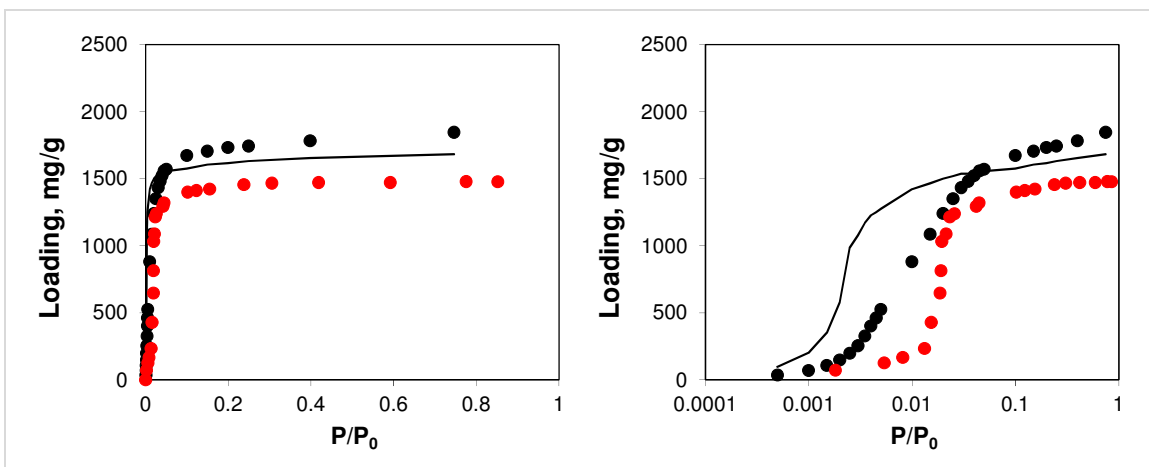


Figure 10. Adsorption isotherms for argon at 78 K in IRMOF-1. Red symbols are the experimental results^{7,26}, black symbols are from molecular simulations, black line corresponds to the system with residual DMF. Panel on the right uses the logarithmic pressure scale.

A natural extension of this approach would be to consider the influence of the residual amounts of other synthetic components, such as terephthalic acid, on adsorption and structural characteristics. It is plausible, that the presence of these components and partially assembled fragments indeed blocks some of the regions of the structure and is behind the differences between the experimental and simulation adsorption behaviour.

Finally, we consider a system where IRMOF-1 structure is doped with several gold nanoclusters. This system belongs to a wider class of MOF structures, where some guest species or objects (nanoparticles, proteins etc) are intentionally trapped inside the cages using either “ship-in-the-bottle” or “ship-around-the-bottle” synthetic strategies (see for example, Refs³⁵⁻³⁸). These systems can lead to new catalytic and sensing devices with exquisite control of accessibility of binding species to the catalytic site or surface, while improving stability of the system due to encapsulation.

For example, in the first article on metal nanoparticles encapsulated in MOFs, Hermes *et al.* used chemical vapour deposition technique (“ship-in-the-bottle”) to prepare copper, palladium and gold nanoparticles inside IRMOF-1³⁹. In case of palladium nanoparticles, their size was around 1.4 nm, while the structure of MOFs has been confirmed to be intact from the X-ray analysis and N₂ sorption experiments. Elemental analysis showed 35.6 wt % metal loading in the structure. In case of gold nanoparticles, TEM and PXRD data indicated polydispersed gold nanoparticles of a much larger size (5-20 nm) at a higher metal loading (48 wt %). It is possible that the gold clusters were forming larger aggregates in these systems across the several cavities. Since this pioneering work, a substantial number of further studies has emerged; however, some of the fundamental issues associated with location, distribution, mobility and accessibility of nanoparticles inside MOF structure remain to be addressed³⁵.

Recently, Vilhelmsen and co-workers employed quantum-mechanical Density Functional Theory (DFT) to understand structure and mobility of gold and palladium clusters (Au₈, Pd₈ and Au₄Pd₄) in MOF-74. One of the key challenges encountered by the authors is the large number of possible stable geometries of adsorbed clusters, which depend on the local environment. For example, it was observed that the structure of the gold cluster in the vicinity of the open metal (zinc) site in MOF-74 is quite different from the most stable structure in the vicinity of the aromatic rings or in the gas phase (on contrary, the most stable structure of the Au₈ cluster near the rings is similar to the most stable gas phase structure). Among other important observations was much stronger adsorption energy for palladium atoms and clusters compared to the gold atoms and clusters. In combination with the analysis of the diffusion barriers, indicating much lower mobility for palladium clusters, this could explain the metal cluster growth and aggregation processes within MOF hosts.

Here we consider a specific case of a small cluster of 13 atoms of gold in fcc arrangement, previously investigated by Zhang *et al.*⁴⁰, using quantum-mechanical density functional theory, in the context of nanoparticles binding to a DNA base. The cluster has diameter of about 8.36 Å, which is slightly smaller than the smallest size of nanoclusters typically reported in experiments (~1 nm). In this work we treat the cluster as a rigid structure,

independent of the environment, which given the results of Vilhelmsen and co-workers is a drastic oversimplification. Several factors may nevertheless somewhat justify this approach as a starting point. Specifically, the most significant deviations of the metal clusters from their stable gas-phase geometries were observed in the vicinity of open metal sites, which are not present in IRMOF-1. In case of adsorption to the locations not involving open metal sites, the deviations from the stable gas-phase geometry were also more significant for the palladium containing clusters. Finally, in the process of translocation along the channel of MOF-74 structure, the geometry of the gold cluster did not change significantly.

Although the size of this nanocluster is slightly larger than the pore limiting diameter in IRMOF-1 ($7.71 \pm 0.20 \text{ \AA}$) the free energy analysis indicates a barrier of only about 7 kJ/mol for this nanocluster to cross the window between two cages of IRMOF-1. Molecular dynamics simulations of 5 clusters in a 2x2x2 system at 300 K (see details in the SI) also confirm this picture: nanoclusters do spend some time in the cages, but on the modest timescale of our simulation (total 2 ns) cross the windows between cages several times. Self-diffusion coefficient of gold nanoclusters is estimated at about $0.18 \cdot 10^{-8} \text{ m}^2/\text{s}$ at 300 K, which is comparable to the self-diffusion coefficient values in IRMOF-1 for smaller species such as cyclohexane⁴¹. This may indicate, that nanoclusters in this work are too small to be properly trapped inside IRMOF-1, however a much more plausible explanation is associated with the deficiency of the employed classical force field. Indeed the lowest adsorption energy observed in this study (-18 kJ/mol) is about five times smaller than that observed for the Au₈ cluster binding to the locations not containing open metal sites in the studies of Vilhelmsen and co-workers (about -98 kJ/mol). Similar difference in the magnitude is also observed for the energy barriers. This indicates that the current classical force field (UFF) significantly underestimates the strength of interaction between metal clusters and structural elements of MOFs. We will return to the developmental needs in the field in the Discussion section.

Five nanoclusters (of 13 atoms each) per eight unit cell of IRMOF-1 correspond to 26 wt % metal loading. From structural analysis, presence of nanoclusters leads to slightly reduced surface area and reduced volume by ~30 % (see SI).

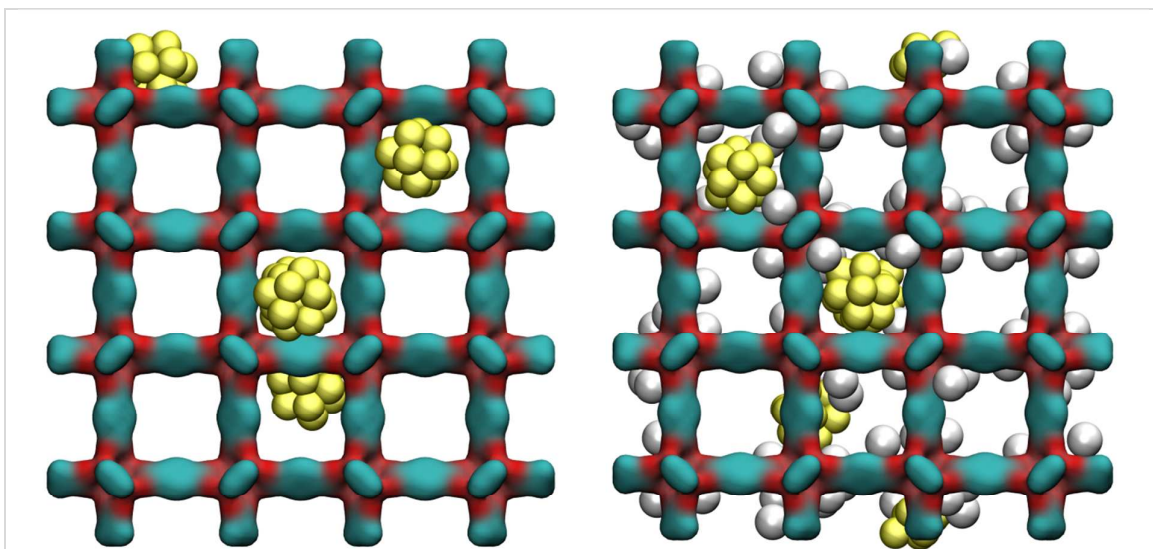


Figure 11. On the left: computer visualization of IRMOF-1 system loaded with gold nanoclusters. On the right: the system is shown together with the adsorbed argon molecules at a low pressure value. Colour scheme: cyan is for carbon, red for oxygen, grey for argon, and yellow for gold, respectively.

As can be seen from Figure 11, at 78 K gold nanoclusters position themselves slightly off-centre of the larger cages, attracted by the linkers. This however does not prevent argon molecules from occupying attractive adsorption sites in the very corner of the cages. Whether this is associated with some displacement of the nanoclusters requires further investigation.

Adsorption behaviour of this system is shown in Figure 12, using both normal and logarithmic scales for pressure.

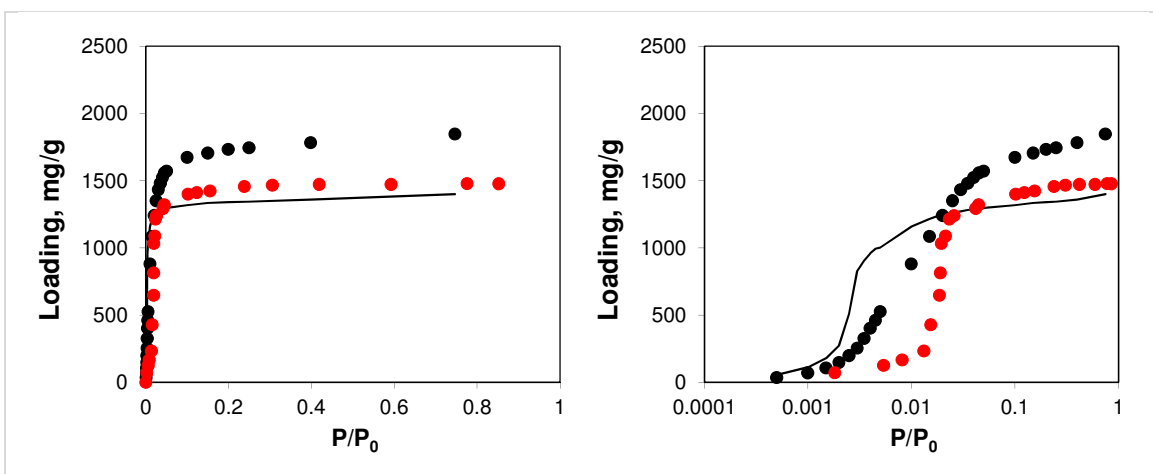


Figure 12. Adsorption isotherms for argon at 78 K. Red symbols are the experimental results^{7, 26}, black symbols are from molecular simulations, black line corresponds to the system loaded with gold nanoclusters. Panel on the right uses the logarithmic pressure scale.

This behaviour is similar to the system with residual DMF molecules: the volume of the system is reduced, while adsorption isotherm is shifted to lower pressures due to the additional interactions resulting from the presence of guest objects. The degree of volume reduction is however greater in the case of gold nanoclusters.

Discussion

Let us recap the main ideas introduced in this article. Understanding the relations between presence of structural defects in MOFs and the resulting properties of MOFs is important for both the development of higher quality, robust crystals and for harvesting new functionalities from these defects. It is difficult to address this problem via experiments only as the very detection and classification of defects is challenging, with several types of defects often present simultaneously in the material.

Thus, experimental efforts must be complemented by molecular simulations and theoretical approaches. Firstly, it is only in molecular simulations where properties of a truly ideal crystal can be obtained, as all real crystals contain defects to some extent. Secondly, within the molecular simulations we can probe a hypothesis on the existence of a particular type of defect and structural disorder by constructing a model featuring this defect and exploring the properties of the resulting structure in comparison with the reference ideal crystal.

The purpose of this article was to illustrate how these models can be constructed using IRMOF-1 as a case study. Specifically, we investigated variants of IRMOF-1 with some of the linkers missing and featuring mesopores. We also considered closely related systems where structural disorder comes from some residual molecules present, or from the encapsulated nanoparticles. The power of molecular simulation comes in the ability to decouple the role of different defects and study their impact in isolation. We focused only on two properties: geometric characteristics of the resulting MOFs and adsorption of argon at cryogenic temperatures.

In particular, these studies show that a structure with as much as 20% of linkers removed can be almost indistinguishable from the ideal structure, as probed by the physical adsorption characterization. However, we expect mechanical and chemical stability of the structure substantially affected by such a concentration of defects. We further show that the shape of the isotherms in the systems featuring mesopores depends substantially on the origin and organization of mesoporosity. Models of this kind can be used to explain recent experimental observations in the systems with sponge-like meso- and macropores. Finally, molecular simulations of the systems featuring additional guest species show the expected decrease in the pore volume (and hence capacity), however, they also provide a wealth of information on the location and mobility of the guest species and on their interactions with the host structure.

This study also highlights the current profound limitations of the classical force fields and simulations. It seems almost all interesting problems associated with the presence of the defects and inclusions in MOFs require some quantum-mechanical level of description!

Indeed, it has been shown that classical potentials and “off-the-shelf” parameters are not able to accurately describe the interactions between guest gas molecules and open metal-sites in MOFs⁴²⁻⁴⁵. Therefore, defects in MOFs, which lead to (greater) exposure of metal atoms, will also need a quantum-mechanical description and the corresponding calibration of the classical potentials. Current classical force fields are not adequate to describe mechanical stability and elastic properties of MOFs (at least, without extensive additional optimization of the parameters), and these problems have been tackled recently using a range of quantum-mechanical tools^{46, 47}. Thus, mechanics of MOFs with defects and guest molecules will also require quantum-mechanical methods. The need for accurate quantum-mechanical approaches to assess the structure and mobility of metal nanoclusters trapped inside MOFs has been already illustrated by Vilhelmsen and co-workers^{48, 49}. Finally, the whole spectrum of problems associated with the catalysis in MOFs, ie breaking and making bonds, again invokes quantum-mechanical methods as the main investigative tool. We are just at the beginning of this new research field and there is a clear need for more extensive and systematic quantum-mechanical exploration of these systems and for the development of accurate, computationally efficient hybrid methods.

Acknowledgements. The author would like to thank Dr David Dubbeldam for the reference adsorption data for argon in IRMOF-1 at 78 K.

References

1. H. Furukawa, K. E. Cordova, M. O’Keeffe and O. M. Yaghi, *Science*, 2013, **341**.
2. H. Furukawa, N. Ko, Y. B. Go, N. Aratani, S. B. Choi, E. Choi, A. O. Yazaydin, R. Q. Snurr, M. O’Keeffe, J. Kim and O. M. Yaghi, *Science*, 2010, **329**, 424-428.
3. G. Ferey and C. Serre, *Chemical Society Reviews*, 2009, **38**, 1380-1399.
4. C. E. Wilmer, M. Leaf, C. Y. Lee, O. K. Farha, B. G. Hauser, J. T. Hupp and R. Q. Snurr, *Nat Chem*, 2011, **4**, 83-89.
5. Z. Fang, B. Bueken, D. E. De Vos and R. A. Fischer, *Angewandte Chemie International Edition*, 2015, **54**, 7234-7254.
6. D. S. Sholl and R. P. Lively, *The Journal of Physical Chemistry Letters*, 2015, **6**, 3437-3444.
7. H. Li, M. Eddaoudi, M. O’Keeffe and O. M. Yaghi, *Nature*, 1999, **402**, 276-279.
8. A. Gupta, S. Chempath, M. J. Sanborn, L. A. Clark and R. Q. Snurr, *Molecular Simulation*, 2003, **29**, 29-46.
9. A. K. Rappe, C. J. Casewit, K. S. Colwell, W. A. Goddard and W. M. Skiff, *Journal of the American Chemical Society*, 1992, **114**, 10024-10035.
10. A. O. Yazaydin, R. Q. Snurr, T. H. Park, K. Koh, J. Liu, M. D. LeVan, A. I. Benin, P. Jakubczak, M. Lanuza, D. B. Galloway, J. J. Low and R. R. Willis, *Journal of the American Chemical Society*, 2009, **131**, 18198-+.
11. C. T. Lee, W. T. Yang and R. G. Parr, *Physical Review B*, 1988, **37**, 785-789.
12. A. D. Becke, *Journal of Chemical Physics*, 1993, **98**, 5648-5652.
13. P. J. Stephens, F. J. Devlin, C. F. Chabalowski and M. J. Frisch, *Journal of Physical Chemistry*, 1994, **98**, 11623-11627.
14. C. M. Breneman and K. B. Wiberg, *Journal of Computational Chemistry*, 1990, **11**, 361-373.
15. Gaussian09.

16. C. J. Fennell and J. D. Gezelter, *Journal of Chemical Physics*, 2006, **124**.
17. P. P. Ewald, *Annalen der Physik*, 1921, **369**, 253-287.
18. J. K. Johnson, J. A. Zollweg and K. E. Gubbins, *Molecular Physics*, 1993, **78**, 591-618.
19. L. Sarkisov and A. Harrison, *Molecular Simulation*, 2011, **37**, 1248-1257.
20. L. Sarkisov, *The Journal of Physical Chemistry C*, 2012, **116**, 3025-3033.
21. L. Sarkisov, *Phys. Chem. Chem. Phys.*, 2012, **14**, 15438-15444.
22. D. Dubbeldam, H. Frost, K. S. Walton and R. Q. Snurr, *Fluid Phase Equilibria*, 2007, **261**, 152-161.
23. K. K. Tanabe and S. M. Cohen, *Chemical Society Reviews*, 2010, **40**, 498-519.
24. H. Deng, C. J. Doonan, H. Furukawa, R. B. Ferreira, J. Towne, C. B. Knobler, B. Wang and O. M. Yaghi, *Science*, 2010, **327**, 846-850.
25. A. G. Wong-Foy, A. J. Matzger and O. M. Yaghi, *Journal of the American Chemical Society*, 2006, **128**, 3494-3495.
26. D. Dubbeldam, H. Frost, K. S. Walton and R. Q. Snurr, *Fluid Phase Equilibria*, 2007, **261**, 152-161.
27. H. Wu, Y. S. Chua, V. Krungleviciute, M. Tyagi, P. Chen, T. Yildirim and W. Zhou, *Journal of the American Chemical Society*, 2013, **135**, 10525-10532.
28. C. V. McGuire and R. S. Forgan, *Chemical Communications*, 2015, **51**, 5199-5217.
29. J. Park, Z. U. Wang, L.-B. Sun, Y.-P. Chen and H.-C. Zhou, *Journal of the American Chemical Society*, 2012, **134**, 20110-20116.
30. M. J. Cliffe, W. Wan, X. Zou, P. A. Chater, A. K. Kleppe, M. G. Tucker, H. Wilhelm, N. P. Funnell, F.-X. Coudert and A. L. Goodwin, *Nat Commun*, 2014, **5**.
31. K. M. Choi, H. J. Jeon, J. K. Kang and O. M. Yaghi, *Journal of the American Chemical Society*, 2011, **133**, 11920-11923.
32. M. Thommes, *Chemie Ingenieur Technik*, 2010, **82**, 1059-1073.
33. M. D. Allendorf, M. E. Foster, F. Léonard, V. Stavila, P. L. Feng, F. P. Doty, K. Leong, E. Y. Ma, S. R. Johnston and A. A. Talin, *The Journal of Physical Chemistry Letters*, 2015, **6**, 1182-1195.
34. Y. S. Bae, D. Dubbeldam, A. Nelson, K. S. Walton, J. T. Hupp and R. Q. Snurr, *Chemistry of Materials*, 2009, **21**, 4768-4777.
35. M. Meilikhov, K. Yussenko, D. Esken, S. Turner, G. Van Tendeloo and R. A. Fischer, *European Journal of Inorganic Chemistry*, 2010, **2010**, 3701-3714.
36. J. Juan-Alcañiz, E. V. Ramos-Fernandez, U. Lafont, J. Gascon and F. Kapteijn, *Journal of Catalysis*, 2010, **269**, 229-241.
37. F. Lyu, Y. Zhang, R. N. Zare, J. Ge and Z. Liu, *Nano Letters*, 2014, **14**, 5761-5765.
38. J. D. Evans, C. J. Sumbly and C. J. Doonan, *Chemical Society Reviews*, 2014, **43**, 5933-5951.
39. S. Hermes, M.-K. Schröter, R. Schmid, L. Khodeir, M. Muhler, A. Tissler, R. W. Fischer and R. A. Fischer, *Angewandte Chemie International Edition*, 2005, **44**, 6237-6241.
40. X. Zhang, C. Q. Sun and H. Hirao, *Physical Chemistry Chemical Physics*, 2013, **15**, 19284-19292.
41. L. Sarkisov, T. Düren and R. Q. Snurr, *Molecular Physics*, 2004, **102**, 211-221.
42. L. J. Chen, L. Grajciar, P. Nachtigall and T. Duren, *Journal of Physical Chemistry C*, 2011, **115**, 23074-23080.
43. L. J. Chen, C. A. Morrison and T. Duren, *Journal of Physical Chemistry C*, 2012, **116**, 18899-18909.
44. M. Fischer, J. R. B. Gomes and M. Jorge, *Molecular Simulation*, 2014, **40**, 537-556.
45. M. Jorge, M. Fischer, J. R. B. Gomes, C. Siquet, J. C. Santos and A. E. Rodrigues, *Industrial & Engineering Chemistry Research*, 2014, **53**, 15475-15487.
46. A. U. Ortiz, A. Boutin, A. H. Fuchs and F. X. Coudert, *Physical Review Letters*, 2012, **109**.
47. L. Chen, J. P. S. Mowat, D. Fairen-Jimenez, C. A. Morrison, S. P. Thompson, P. A. Wright and T. Duren, *Journal of the American Chemical Society*, 2013.

48. L. B. Vilhelmsen, K. S. Walton and D. S. Sholl, *Journal of the American Chemical Society*, 2012, **134**, 12807-12816.
49. L. B. Vilhelmsen and D. S. Sholl, *Journal of Physical Chemistry Letters*, 2012, **3**, 3702-3706.